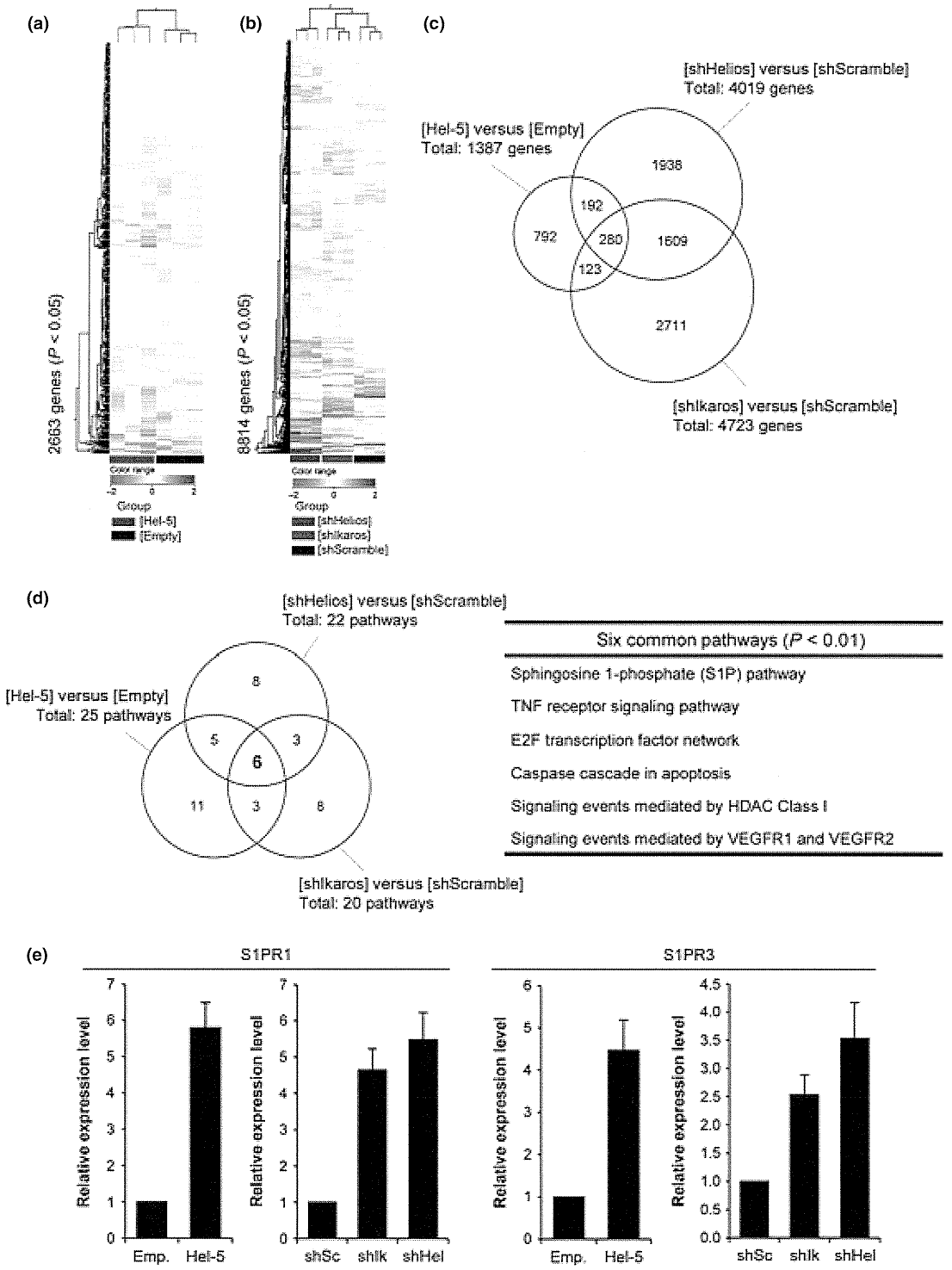

Fig. 7. Comprehensive search for Helios target genes by microarray analysis. (a,b) Gene expression analysis of Jurkat stable cells. The gene expression patterns of Jurkat cells expressing Hel-5 (n = 3), shIkaros (n = 3), and shHelios (n = 3) were comprehensively analyzed by microarray technique. The obtained 2D hierarchical clusters and Pearson's correlation between the cells expressing Hel-5 or not (a) and the cells introducing shHel, shIk, or shSc (b). (c) Venn diagram of differential gene expression pattern in the Jurkat sublines. The each differential expression gene set (5-fold changes, $P < 1 \times 10^{-5}$) was compared. (d) Venn diagram depicting the overlap between the outputs of pathway analysis in Jurkat sublines. The analysis was based on the NCI-Nature Pathway Interaction Database.[37] Each differential pathway set (t-test, $P < 0.01$) was compared and the common pathways listed. (e) Results of quantitative RT-PCR of shingosine-1-phosphate receptor 1 (S1PR1) and receptor 3 (S1PR3) in Jurkat sublines (n = 3, mean ± SD). HDAC, histone deacetylase; VEGFR, vascular endothelial growth factor receptor.

Acknowledgments

We thank Mr. M. Nakashima and Ms. T. Akashi for support and maintenance of the Joint Study on Prognostic Factors of ATL Development. This work is supported by JSPS KAKENHI Grant Numbers 24790436 (M.Y.), 23390250 (T.W.), 23659484 (T.W.), 23 6291 (S.A.), NEXT KAKENHI Grant Number 221S0001 (T.W.), and a Grant-in-Aid from the Ministry of Health, Labor and Welfare of Japan H24-G-004 (M.Y. and T.W.).

doi: 10.1111/cas.12181

Disclosure Statement

The authors have no conflict of interest.

References

1 Yamaguchi K, Watanabe T. Human T lymphotropic virus type-I and adult T-cell leukemia in Japan. *Int J Hematol* 2002; **76**: 240–45.
2 Iwanaga M, Watanabe T, Utsunomiya A *et al.* Human T-cell leukemia virus type I (HTLV-1) proviral load and disease progression in asymptomatic HTLV-1 carriers: a nationwide prospective study in Japan. *Blood* 2010; **116**: 1211–19.
3 Yamagishi M, Nakano K, Miyake A *et al.* Polycomb-mediated loss of miR-31 activates NIK-dependent NF-κB pathway in adult T cell leukemia and other cancers. *Cancer Cell* 2012; **21**: 121–35.
4 Yamagishi M, Watanabe T. Molecular hallmarks of adult T cell leukemia. *Front Microbiol* 2012; **3**: 334.
5 Lo K, Landau NR, Smale ST. LyF-1, a transcriptional regulator that interacts with a novel class of promoters for lymphocyte-specific genes. *Mol Cell Biol* 1991; **11**: 5229–43.
6 Georgopoulos K, Moore DD, Derfler B. Ikaros, an early lymphoid-specific-transcription factor and a putative mediator for T cell commitment. *Science* 1992; **258**: 808–12.
7 Hahm K, Ernst P, Lo K, Kim GS, Turck C, Smale ST. The lymphoid transcription factor LyF-1 is encoded by specific, alternatively spliced mRNAs derived from the Ikaros gene. *Mol Cell Biol* 1994; **14**: 7111–23.
8 Sun L, Liu A. Zinc finger-mediated protein interactions modulate Ikaros activity, a molecular control of lymphocyte development. *EMBO J* 1996; **15**: 5358–69.
9 Morgan B, Sun L, Avitahl N *et al.* Aiolos, a lymphoid restricted transcription factor that interacts with Ikaros to regulate lymphocyte differentiation. *EMBO J* 1997; **16**: 2004–13.
10 Kelley CM, Ikeda T, Koipally J *et al.* Helios, a novel dimerization partner of Ikaros expressed in the earliest hematopoietic progenitors. *Curr Biol* 1998; **8**: 508–15.
11 Cobb BS, McCarty AS, Brown KE *et al.* Helios, a T cell-restricted Ikaros family member that quantitatively associates with Ikaros at centromeric heterochromatin. *Genes Dev* 1998; **12**: 782–96.
12 Winandy S, Wu P, Georgopoulos K. A dominant mutation in the Ikaros gene leads to rapid development of leukemia and lymphoma. *Cell* 1995; **83**: 289–99.
13 Wang JH, Nichogiannopoulou A, Wu L *et al.* Selective defects in the development of the fetal and adult lymphoid system in mice with an Ikaros null mutation. *Immunity* 1996; **5**: 537–49.
14 Wang JH, Avitahl N, Cariappa A *et al.* Aiolos regulates B cell activation and maturation to effector state. *Immunity* 1998; **9**: 543–53.
15 Zhang Z, Swindle CS, Bates JT, Ko R, Cotta CV, Klug CA. Expression of a non-DNA-binding isoform of Helios induces T-cell lymphoma in mice. *Blood* 2007; **109**: 2190–7.
16 Sun L, Crotty ML, Sensel M *et al.* Expression of dominant-negative Ikaros isoforms in T-cell acute lymphoblastic leukemia. *Clin Cancer Res* 1999; **5**: 2112–20.
17 Nakase K, Ishimaru F, Avitahl N *et al.* Dominant negative isoform of the Ikaros gene in patients with adult B-cell acute lymphoblastic leukemia. *Cancer Res* 2000; **60**: 062–4065.
18 Takanashi M, Yagi T, Imamura T *et al.* Expression of the Ikaros gene family in childhood acute lymphoblastic leukaemia. *Br J Haematol* 2002; **117**: 525–30.
19 Nishii K, Katayama N, Miwa H. Non-DNA-binding Ikaros isoform gene expressed in adult B-precursor acute lymphoblastic leukemia. *Leukemia* 2002; **16**: 1285–92.
20 Tonnelle C, Imbert M-C, Sainty D, Granjeaud S, N'Guyen C, Chabannon C. Overexpression of dominant-negative Ikaros 6 protein is restricted to a subset of B common adult acute lymphoblastic leukemias that express high levels of the CD34 antigen. *Hematol J* 2003; **4**: 104–9.
21 Klein F, Feldhahn N, Herzog S *et al.* BCR-ABL1 induces aberrant splicing of IKAROS and lineage infidelity in pre-B lymphoblastic leukemia cells. *Oncogene* 2006; **25**: 1118–24.
22 Zhou F, Mei H, Jin R, Li X, Chen X. Expression of ikaros isoform 6 in chinese children with acute lymphoblastic leukemia. *J Pediatr Hematol Oncol* 2011; **33**: 429–32.
23 Mullighan CG, Miller CB, Radtke I *et al.* BCR-ABL1 lymphoblastic leukaemia is characterized by the deletion of Ikaros. *Nature* 2008; **453**: 110–14.
24 Kano G, Morimoto A, Takanashi M *et al.* Ikaros dominant negative isoform (Ik6) induces IL-3-independent survival of murine pro-B lymphocytes by activating JAK-STAT and up-regulating Bcl-xl levels. *Leuk Lymphoma* 2008; **49**: 965–73.
25 Iacobucci I, Lonetti A, Messa F *et al.* Expression of spliced oncogenic Ikaros isoforms in Philadelphia-positive acute lymphoblastic leukemia patients treated with tyrosine kinase inhibitors: implications for a new mechanism of resistance. *Blood* 2008; **112**: 3847–55.
26 Mullighan CG, Su X, Zhang J *et al.* Deletion of IKZF1 and prognosis in acute lymphoblastic leukemia. *N Engl J Med* 2009; **360**: 470–80.
27 Kuiper RP, Waanders E, van der Velden VHJ *et al.* IKZF1 deletions predict relapse in uniformly treated pediatric precursor B-ALL. *Leukemia* 2010; **24**: 1258–64.
28 Nakase K, Ishimaru F, Fujii K *et al.* Overexpression of novel short isoforms of Helios in a patient with T-cell acute lymphoblastic leukemia. *Exp Hematol* 2002; **30**: 313–17.
29 Fujii K, Ishimaru F, Tabayashi T *et al.* Over-expression of short isoforms of Helios in patients with adult T-cell leukaemia/lymphoma. *Br J Haematol* 2003; **120**: 986–9.
30 Fujiwara SI, Yamashita Y, Nakamura N *et al.* High-resolution analysis of chromosome copy number alterations in angioimmunoblastic T-cell lymphoma and peripheral T-cell lymphoma, unspecified, with single nucleotide polymorphism-typing microarrays. *Leukemia* 2008; **22**: 1891–8.
31 Fujimoto R, Ozawa T, Itoyama T, Sadamori N, Kurosawa N, Isobe M. HELIOS-BCL11B fusion gene involvement in a t(2;14)(q34;q32) in an adult T-cell leukemia patient. *Cancer Genet* 2012; **205**: 356–64.
32 Shimoyama M. Diagnostic criteria and classification of clinical subtypes of adult T-cell leukaemia-lymphoma. A report from the Lymphoma Study Group (1984–87). *Br J Haematol* 1991; **79**: 428–37.
33 Tabayashi T, Ishimaru F, Takata M *et al.* Characterization of the short isoform of Helios overexpressed in patients with T-cell malignancies. *Cancer Sci* 2007; **98**: 182–8.
34 Kathrein KL, Chari S, Winandy S. Ikaros directly represses the notch target gene Hes1 in a leukemia T cell line: implications for CD4 regulation. *J Biol Chem* 2008; **283**: 10476–84.
35 Kleinmann E, Geimer Le Lay AS, Sellars M, Kastner P, Chan S. Ikaros represses the transcriptional response to Notch signaling in T-cell development. *Mol Cell Biol* 2008; **28**: 7465–75.
36 Molnár A, Georgopoulos K. The Ikaros gene encodes a family of functionally diverse zinc finger DNA-binding proteins. *Mol Cell Biol* 1994; **14**: 8292–303.
37 Schaefer CF, Anthony K, Krupa S *et al.* PID: the pathway interaction database. *Nucleic Acids Res* 2009; **37**: D674–9.
38 Pancewicz J, Taylor JM, Datta A. Notch signaling contributes to proliferation and tumor formation of human T-cell leukemia virus type 1-associated adult T-cell leukemia. *Proc Natl Acad Sci USA* 2010; **107**: 16619–24.
39 Murata K, Hattori M, Hirai N *et al.* Hes1 directly controls cell proliferation through the transcriptional repression of p27Kip1. *Mol Cell Biol* 2005; **25**: 4262–71.
40 Maeda Y, Seki N, Sato N, Sugahara K, Chiba K. Sphingosine 1-phosphate receptor type 1 regulates egress of mature T cells from mouse bone marrow. *Int Immunol* 2010; **22**: 515–25.
41 Spiegel S, Milstien S. The outs and the ins of sphingosine-1-phosphate in immunity. *Nat Rev Immunol* 2011; **11**: 403–15.
42 Maceyka M, Harikumar KB, Milstien S, Spiegel S. Sphingosine-1-phosphate signaling and its role in disease. *Trends Cell Biol* 2012; **22**: 50–60.
43 Ghigna C, Valacca C, Biamonti G. Alternative splicing and tumor progression. *Curr Genomics* 2008; **9**: 556–70.
44 David CJ, Manley JL. Alternative pre-mRNA splicing regulation in cancer: pathways and programs unhinged. *Genes Dev* 2010; **24**: 2343–64.
45 Blair CA, Zi X. Potential molecular targeting of splice variants for cancer treatment. *Indian J Exp Biol* 2011; **49**: 836–9.

Supporting Information

Additional Supporting Information may be found in the online version of this article:

Fig. S1. Deregulated expression of Ikaros family genes in primary adult T-cell leukemia cells.

Fig. S2. Colocalization of wild-type Ikaros and adult T-cell leukemia-type Helios.

Fig. S3. Dominant-negative inhibition of Hel-6, Hel-v1, and Hel-v2 in the suppressive activities of wild-type Helios and Ikaros.

Fig. S4. Downregulation of the expression of Helios mRNA in HTLV-1-positive T cell lines.

Fig. S5. Overexpression of abnormal Helios isoforms lacking exon 6 in adult T-cell leukemia samples.

Fig. S6. Relative value of Helios transcripts skipping exon 3 to all is upregulated in primary adult T-cell leukemia cells.

Fig. S7. Upregulated expression of Hes1 in primary adult T-cell leukemia cells.

Table S1. Clinical characteristics of adult T-cell leukemia patients and HTLV-1 carriers.

Table S2. Primer list and probe sequences.

doi: 10.1111/cas.12181

THE PROTEIN SOCIETY

Effects of subclass change on the structural stability of chimeric, humanized, and human antibodies under thermal stress

Takahiko Ito,[1,2,3] and Kouhei Tsumoto[2,3,4,5]*

[1]Bio Process Research and Development Laboratories, Production Division, Kyowa Hakko Kirin Company Limited, 100-1 Hagiwara-machi, Takasaki, Gunma, 370-0013, Japan

[2]Institute of Medical Science, The University of Tokyo, 4–6-1 Shirokanedai, Minato-ku, Tokyo, 108–8639, Japan

[3]Department of Medical Genome Sciences, Graduate School of Frontier Sciences, , The University of Tokyo, Kashiwa, 277–8562, Japan

[4]Department of Chemistry and Biotechnology, School of Engineering, The University of Tokyo, Tokyo, 113-0024, Japan

[5]Department of Bioengineering, School of Engineering, The University of Tokyo, Tokyo, 113-0024, Japan

Received 23 June 2013; Accepted 6 August 2013
DOI: 10.1002/pro.2340
Published online 21 August 2013 proteinscience.org

Abstract: To address how changes in the subclass of antibody molecules affect their thermodynamic stability, we prepared three types of four monoclonal antibody molecules (chimeric, humanized, and human) and analyzed their structural stability under thermal stress by using size-exclusion chromatography, differential scanning calorimetry (DSC), circular dichroism (CD), and differential scanning fluoroscopy (DSF) with SYPRO Orange as a dye probe. All four molecules showed the same trend in change of structural stability; the order of the total amount of aggregates was IgG1 < IgG2 < IgG4. We thus successfully cross-validated the effects of subclass change on the structural stability of antibodies under thermal stress by using four methods. The T_h values obtained with DSF were well correlated with the onset temperatures obtained with DSC and CD, suggesting that structural perturbation of the CH2 region could be monitored by using DSF. Our results suggested that variable domains dominated changes in structural stability and that the physicochemical properties of the constant regions of IgG were not altered, regardless of the variable regions fused.

Keywords: antibody; circular dichroism; differential scanning calorimetry; differential scanning fluoroscopy; subclass change; thermodynamic stability

Abbreviations: CD, circular dichroism; DSC, differential scanning calorimetry; DSF, differential scanning fluoroscopy; DTT, dithiothreitol; HMWS, high-molecular-weight species; LMWS, low-molecular-weight species; MRW, mean residue weight; SEC, size-exclusion chromatography; VH, variable regions of heavy chains; VL, variable regions of light chains.

Additional Supporting Information may be found in the online version of this article.

Grant sponsor: Japanese Society of the Promotion of Science,. Grant sponsor: World-Leading Innovative R&D on Science and Technology (FIRST Program) from Council for Science and Technology Policy (CSTP).

*Correspondence to: Kouhei Tsumoto, Institute of Medical Science, The University of Tokyo, 4–6-1 Shirokanedai, Minato-ku, Tokyo 108–8639, Japan. E-mail: tsumoto@ims.u-tokyo.ac.jp

Introduction

Monoclonal antibodies (mAbs) are very versatile reagents and are under extensive development for therapeutic use. To date, more than 30 therapeutic antibodies have been approved for clinical use and more than 240 molecules are under development.[1–3]

Antibodies are heterodimers composed of two heavy chains and two light chains, which are linked through disulfide bonds. As classified on the basis of the constant region of the heavy chain there are five classes of antibody, namely IgA, IgD, IgE, IgG, and IgM. The constant heavy regions of IgA, IgD, and IgG have three IgG domains and a hinge region to

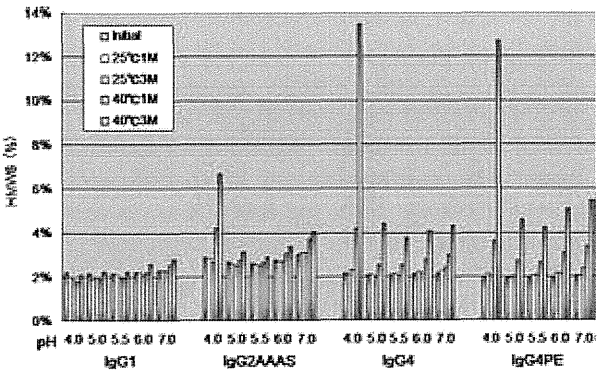

Figure 1. Size-exclusion high-performance liquid chromatographic analysis of percentages of HMWS as a function of pH after storage at 25 or 40°C for 1 or 3 months.

give flexibility. Despite this range of choice of antibody classes to select from in the development of therapeutic antibodies, all recombinant antibodies under development to date have belonged to the IgG class because it has the highest serum half-life among all the classes.[4,5]

Four subclasses of IgG antibody have been identified, and each subclass has, in principle, highly homologous constant region sequences. However, the abilities of the IgGs in the four subclasses to trigger effector functions differ distinctly. For therapeutic applications the subclass needs to be carefully chosen; to achieve the desired therapeutic effects and avoid side effects, subclass selection is primarily dictated by the effector functions needed. IgG1 and IgG3 have greater ability to activate antibody-dependent cellular cytotoxicity and complement-dependent cellular cytotoxicity than do IgG2 and IgG4.[6–8] If the effector function is required to eliminate targets (e.g., to destroy tumor cells in oncology applications), one would expect IgG1 or IgG3 to be used. However, in practice, the IgG3 subclass has not been used as a therapeutic candidate owing to its short half-life and long hinge region, which makes it susceptible to proteolysis, along with its allotypic polymorphism.[9] Most of the therapeutic antibodies approved to date have belonged to the IgG1 subclass; only a few IgG2 and IgG4 antibodies have reached the market.[3] Nevertheless, subclasses IgG2 and IgG4 are increasingly being developed as therapeutic antibodies because of their blocking or inhibitory functions.[9] Selection of antibody subclass is therefore considered increasingly critical in the development of therapeutic antibodies.[9]

Products have been developed that have reduced effector functions compared with those seen with the IgG1 subclass.[10–12] IgG2 and IgG4 have unique physicochemical properties. Human IgG2 antibodies can form covalent dimers and structural isoforms via disulfide shuffling *in vivo*.[13–17] IgG4 antibodies can form half-antibodies (i.e., those with one heavy chain and one light chain) that lack inter-heavy chain disulfide bonds and form intra-chain disulfide bonds. Recent studies have shown that a half-antibody can exchange with another IgG4 half-antibody, resulting in the production of a bispecific antibody.[18–20] Moreover, IgG2 and IgG4 are unstable in terms of tendency to aggregate.[21,22] Among the physicochemical properties of antibodies, homogeneity and stability are particularly critical issues limiting the successful development of therapeutic antibodies.

Here, we focus on the effects of changes in IgG subclass on the conformational and physicochemical stability of antibodies. We prepared three types of four antibody molecules, namely chimeric, humanized, and human. From our results, we concluded that changes in variable domains dominate changes in thermodynamic stability and that the trends in thermodynamic stability caused by changes due to subclass switching are in principle identical among antibody molecules.

Results

Size-exclusion chromatography and SDS-PAGE

To compare differences in aggregation and degradation tendency among subclasses, we investigated aggregation and degradation behavior in the pH range of 4.0–7.0 at 25°C and 40°C. Samples taken at different incubation times were analyzed by using size-exclusion chromatography (SEC).

We tried to construct and analyze subclass-substituted molecules of mAb-A, mAb-B, mAb-C, and mAb-D. Here, we first give the results for mAb-C, followed by those of the other antibody molecules.

Supporting Information Figures 1 to 1–6 give representative SEC chromatograms of mAb-C (chromatographic UV profile) for various glutamate formulations as a function of pH. The intact non-aggregated antibody (monomer) was eluted at approximately 31.5 min. Soluble aggregate (high-molecular-weight species, HMWS) was eluted earlier, and degraded species (low-molecular-weight species, LMWS) were eluted later. The total amounts of degraded species were enhanced with increasing incubation time at 40°C.

All subclasses were most stable at pH 5.5, and the total HMWS content was enhanced with increasing pH in the range 5.5–7.0. In the case of IgG1, the lower pH samples exhibited greater physical stability, as evidenced by less aggregation. In contrast, IgG2AAAS, IgG4, and IgG4PE showed greater aggregation at lower pH (pH 4.0 and 5.5).

We examined the percentages of HMWS, as revealed by SEC analysis as a function of pH after storage at 25°C or 40°C for 1 or 3 months (Fig. 1). IgG1 showed no increase in HMWS content over time at pH 4.0 at 40°C from time zero (Initial) to 3

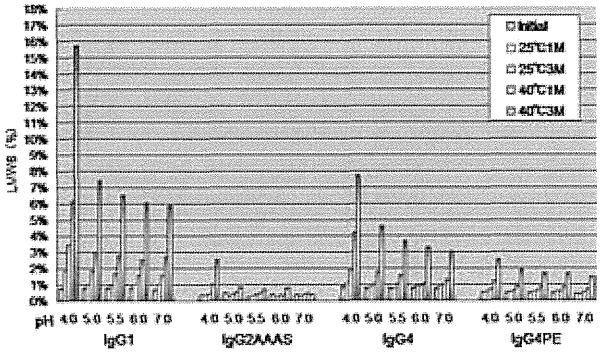

Figure 2. Size-exclusion high performance liquid chromatographic analysis of percentages of LMWS as a function of pH after storage at 25 or and 40°C for 1 or 3 months.

months. In contrast, IgG2 (IgG2AAAS) and IgG4 (IgG4PE) showed an increase in HMWS content over time at 40°C during the 3-month period at all pH values. The rate of aggregation was strongly dependent on the antibody subclass (IgG1 vs. IgG2 vs. IgG4). At 40°C, all IgG1s were resistant to low-pH aggregation, but the IgG2s and IgG4s were aggregated.

We examined the percentages of LMWS, as revealed by SEC analysis as a function of pH after storage at 25°C or 40°C for 1 or 3 months (Fig. 2). All subclasses were most stable at pH 5.5–6.0 and showed decreasing LMWS content with increasing pH in the range 4.0–6.0. IgG1 samples exhibited more LMWS than did IgG2 and IgG4 samples, revealing the lower chemical stability of IgG1. The amount of LMWS was highest at pH 4.0 for each subclass, although to differing extents. Reducing and non-reducing SDS-PAGE showed a high-molecular-weight ladder (data not shown); this was consistent with the heterogeneity observed within the aggregates upon SEC.

The same trend was observed for other antibodies: examples for mAb-D are given in Supporting Information Figure 1 (1-7 to 1–11).

Differential scanning calorimetry

To determine whether antibodies of different subclasses exhibited different thermodynamic stabilities, we obtained differential scanning calorimetry (DSC) thermograms for antibodies of three different subclasses, including mutations that had the same variable region. We constructed and analyzed subclass-substituted molecules of mAb-A, mAb-B, mAb-C, and mAb-D. Here, we first describe the results for mAb-C, followed by a discussion of the other mutants.

We examined the profiles of temperature-induced unfolding of all subclasses of mAb-C (IgG1, IgG2AAAS, IgG4, IgG4PE) under the same solvent conditions (Fig. 3). Table 1 lists the observed thermal unfolding midpoint (T_m) values for mAb-C. In the case of mAb-C, we prepared IgG1, IgG2AAAS, IgG4, and IgG4PE. Thermal unfolding of mAb-C G1 resulted in three partially overlapping transitions with T_m values of about 73, 78, and 84°C, respectively, at pH 5.5 under optimized formulation conditions. The results showed good agreement with previous results from an IgG1 Mab, in which the three transitions were assigned to unfolding of the CH2 domain, the antigen-binding fragment (Fab), and the CH3 domain.[23,24] For mAb-C G2AAAS, G4, and G4PE, the first transition shifted to the low temperature side compared with that for IgG1. The change in the number of transitions in members of the IgG subclass with the same variable regions of heavy and light chains (VH/VL region) suggests that independent unfolding of the CH2, CH3, and Fab domains is a general property of IgGs.

The apparent Fab T_m values of mAb-C in the IgG1 and IgG2AAAS formats were similar to each other ($\Delta T_m < 0.3$°C), whereas the apparent Fab T_m values in the IgG4 and IgG4PE formats were about 1°C different from the Fab T_m values of mAb-C in the IgG1 and IgG2AAAS formats. Among the four antibodies with the same variable domains and different subclasses, the T_m values of the Fab fragments differed in the order of IgG1 ≥ IgG2 ≥ IgG4 and IgG4PE.

The same trend was observed for the other antibodies, namely mAb-A, mAb-B, and mAb-D: a list of observed T_m values is given in Supporting Information Tables 1–III and Supporting Information Figure 2. Average values of T_m for the four antibodies were calculated and plotted against pH (Fig. 4). The CH1 and Fc sequences of the IgG subclasses have some amino acid differences and different disulfide-bonding patterns (data not shown); this might suggest why the effects on the profiles of antibodies with different variable domains were identical.

Changing pH had marked effects on the DSC profiles of each antibody molecule reported here (Table 1, Supporting Information Tables 1–III). A decrease in pH resulted in broader endotherms that occurred at lower temperatures. Notably, the CH2

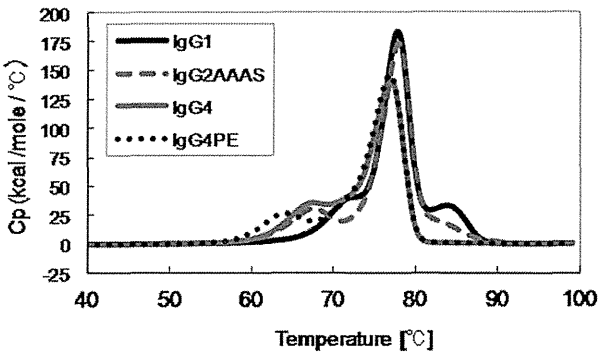

Figure 3. Temperatures inducing melting (unfolding) of all subclasses of mAb-C at pH 5.5, as measured by using DSC.

Table 1. *Differential scanning calorimetry measurements of melting transition of mAb-C in all subclasses as a function of pH.*

			Tm (°C)				
Subclass	domain	pH	4.0	5.0	5.5	6.0	7.0
G1							
	CH2		60.10	69.41	72.55	73.23	73.72
	Fab		73.91	77.23	77.87	78.05	78.06
	CH3		79.07	83.55	83.88	84.05	84.02
G2AAAS							
	CH2		52.78	64.55	67.73	69.24	70.50
	Fab		72.58	77.19	78.04	77.58	77.99
	CH3		NA	NA	NA	NA	NA
G4							
	CH2		54.76	64.07	67.40	69.04	69.90
	Fab		71.07	76.55	77.05	76.36	76.06
	CH3		NA	NA	NA	NA	NA
G4PE							
	CH2		53.77	61.42	64.08	65.79	67.74
	Fab		71.25	76.55	76.90	76.27	75.56
	CH3		NA	NA	NA	NA	NA

NA, not available; melting transition was not detected or well defined.

domain displayed greater pH dependence of thermal stability than did the CH3 domain; ΔT_m was larger for IgG4 than for IgG1 and IgG2.

Previous characterization of the Fc fragment has identified an early transition due to unfolding of the CH2 domain followed by thermal unfolding of the CH3 domain.[25] Previous studies indicate that the CH3 region of IgG1 has an extremely high T_m compared with other domains.[25] Of the three human IgG subclasses (IgG1, IgG2, and IgG4), IgG1 has the most stable Fc, based on the T_m of its CH2 and CH3 domain.[24] This subclass dependence is correlated with reduced thermodynamic stability of IgG2 and IgG4 CH2 relative to IgG1 CH2. Regardless of subclass, we found that thermodynamic stability of CH2 was an important determinant of the stability and aggregation of Fc and intact antibody molecules under acidic conditions. Some of these findings have already been reported.[26,27] Notably, also, the unfolding transitions of the CH2 and CH3 domains for all four IgG1 constructs were identical as described in the results. This trend was also observed for the other subclasses, namely IgG2, IgG2AAAS, IgG4, and IgG4PE; in contrast, the Fab unfolding transitions were highly variable.

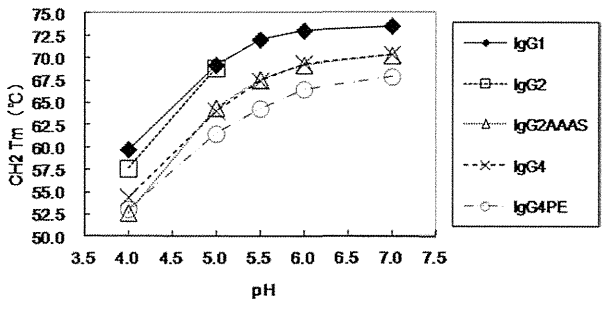

Figure 4. DSC measurements of CH2-domain melting transition of antibodies as a function of pH. IgG1, 4 (mAb-A, B, C, D); IgG2, 2 (mAb-A, -B); IgG2AAAS, 2 (mAb-C, -D); IgG4, 2 (mAb-C, -D); IgG4PE, 4 (mAb-A, -B, -C, -D).

Circular dichroism

We used far-UV circular dichroism (CD) to compare the secondary structures of the subclasses (Supporting Information Figs. 3-1 to 3-3). First, we give the results for mAb-C, followed by a discussion of those for the other antibody molecules.

The CD spectra of all subclasses of mAb-C before and after heating are shown in Supporting Information Figure 3-1. The subclasses showed little difference in terms of far-UV CD before heating (Supporting Information Fig. 3-1a), regardless of pH (data not shown). The spectra were characterized by a single negative peak with a minimum at a wavelength of 217 nm, suggestive of the expected β-sheet structure of the immunoglobulin fold.[28] These observations suggested that subclass changes did not alter the overall secondary structure.

To probe the thermal stability, we monitored the signal at 217 nm from 25 to 100°C and compared the thermal stabilities of the subclasses (Fig. 5). In all of the ellipticity–temperature profiles there were two steps at which the intensity decreased, suggesting that there were two distinct temperatures at which changes in secondary structure occurred. At pH 4.0, the antibody had a slightly lower transition-onset temperature than at other pH values. The transition-onset temperatures of the antibody at pH 5.0 and 6.0 were comparable, and the ellipticity did not change until the temperature reached approximately 60°C, whereas a much lower onset temperature was observed at pH 4.0. At pH 4.0, the major

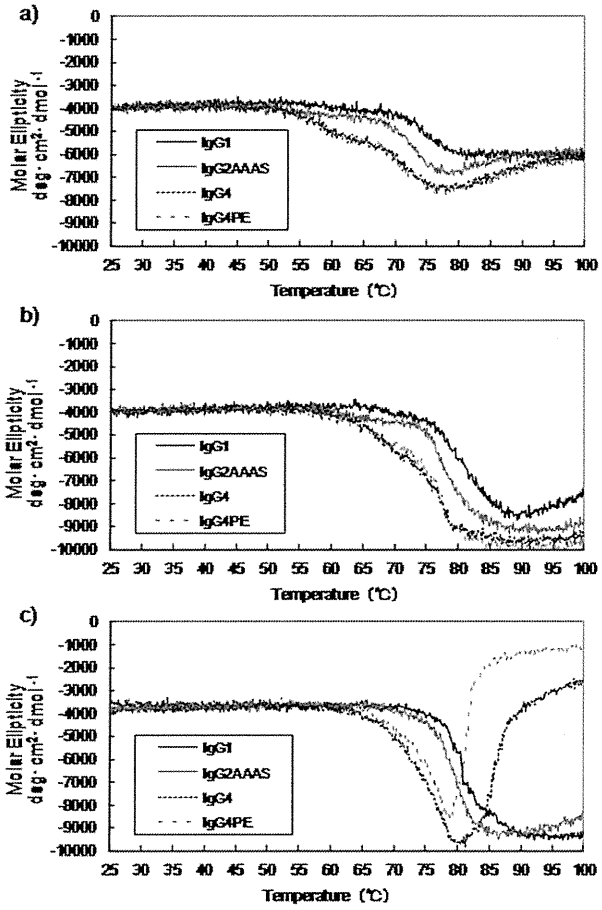

Figure 5. Effect of temperature and pH on molar ellipticity at a wavelength of 217 nm (a, pH 4.0; b, pH 5.5; c, pH 6.0) in the case of mAb-C.

changes occurred at 55°C, followed by a second step at about 70°C, in all subclasses. The transition-onset temperatures were in the order of IgG4 < IgG2 < IgG1. Furthermore, in the case of the IgG4 formats, precipitation was observed after heating at pH 6.0. The temperature values corresponded well to the T_m values observed for the structural transitions in the DSC experiments. IgG4 has the lowest thermal stability among the subclasses reported here.

Next, we obtained CD spectra of different subclasses of the other three antibodies, mAb-A, mAb-B, and mAb-D; the results for mAb-A and mAb-D are shown in Supporting Information Figures 3-2, 3-3 and 4-1, 4-2, respectively. The same trends as with mAb-C were observed for these antibodies.

Differential scanning fluoroscopy

The typical differential scanning fluoroscopy (DSF) profile of an IgG molecule consists of a sharp sigmoid-like increase to the maximum level, followed by a decrease in fluorescence intensity. This profile represents changes in the environment of the dye. The initial increase in fluorescence most likely results from exposure of the dye to the hydrophobic area of the protein during thermal unfolding; the degree of exposure depends on the rate of transition from the folded to the unfolded state. Fluorescence quenching at increased solution temperature—a nonspecific transition—also occurs and contributes to the overall sigmoidal shape.[29–31] Here, we used SYPRO Orange as a probe in the DSF system.

We investigated four mAb molecules: mAb-A and mAb-B (IgG1, IgG2, IgG4PE) and mAb-C and mAb-D (IgG1, IgG2AAAS, IgG4, IgG4PE). We used a variety of formulation pH values to generate DSF profiles for each mAb's subclasses.

Here, we give the results for mAb-C as an example. The fluorescence profiles and temperatures of hydrophobic exposure (T_h) of each subclass-changed IgG are shown in Supporting Information Figures 5-1 to 5-5 and Table II, respectively. Comparison of fluorescence profiles at pH 5.5 revealed that the fluorescence intensity increased at about 55°C; after two-step transitions it then decreased at about 80°C. These findings were similar to the results reported previously.[29,30] The changes in intensity started in the order of IgG4PE, IgG4, IgG2AAAS, and IgG1. IgG1 had the highest Th1 value, followed by IgG2AAAS, IgG4, and IgG4PE. The order was almost the same in the case of the Th2 values.

Next, we examined the effects of pH on changes in Th1 and Th2 values. In all subclass-changed IgGs the Th1 and Th2 values were highest at neutral pH; a decrease in pH led to a decrease in values. Notably, our DSF analyses showed that mutations into IgG2 and IgG4 led to decreases in T_h values, and that the Th1 value of IgG2AAAS at pH 4.0 was lower than that of IgG4. These results are in good accordance with those obtained from DSC. The trends were similar for the other mAbs.

Discussion

Here, we reported the effects of changes in antibody subclass on stability in terms of molecule conservation and on structural stability. We focused on four antibody molecules (chimeric, humanized, and human), and three subtypes were constructed for each of the four antibodies. We substituted another subclass for the constant region of each antibody. These subclass-changed molecules had the same variable domains but different constant regions; we could therefore evaluate how subclass affected the physicochemical properties of IgG.

The results of SEC and SDS-PAGE revealed clear differences in the physical and chemical degradation of various IgGs. IgG1s were more susceptible to fragmentation, whereas IgG2s and IgG4s were more susceptible than IgG1 to aggregation at low pH. Degradation of human IgG1 at low pH originates from non-enzymatic digestion of the upper hinge region (i.e., EPKSCDKTHT; digested site is

Table II. *Temperature of Hydrophobic Exposure (T_h) Values of Antibodies Obtained From Differential Scanning Fluoroscopy Measurements, as a Function of pH*

		Tm (°C)				
Subclass	pH	4.0	5.0	5.5	6.0	7.0
Mab-A						
G1						
	Th1	63	68	69.5	70	70.5
	Th2	73	74.5	74.5	NA	NA
G2						
	Th1	62.5	68	69.5	70	70.5
	Th2	71.5	73	NA	NA	NA
G4PE						
	Th1	56.5	60	61	61.5	62
	Th2	67.5	69.5	70	70	70
Mab-B						
G1						
Mab-C						
G1						
	Th1	62.5	67.5	69	69.5	70
	Th2	74	75	75	74.5	74
G2						
	Th1	61.5	67	69	70	70.5
	Th2	73.5	74.5	74.5	74.5	NA
G4PE						
	Th1	56.5	60	60.5	61	62
	Th2	73	74	74	73.5	73.5
Mab-C						
G1						
	Th1	63.5	68	69.5	70	70.5
	Th2	76.5	78	78	78	78
G2AAAS						
	Th1	58.5	63.5	65	66	66
	Th2	74.5	76.5	77	77.5	77.5
G4						
	Th1	59	62.5	64	65	65.5
	Th2	74	75.5	76	76	75.5
G4PE						
	Th1	56.5	60.5	61.5	62	62.5
	Th2	74	75.5	75.5	75.5	75.5
Mab-D						
G1						
	Th1	63	68	69	70	70
	Th2	79	81	81.5	82	82.5
G2AAAS						
	Th1	58	63	65	65.5	66
	Th2	75	82.5	82.5	83	83
G4						
	Th1	58	62.5	64.5	65.5	65.5
	Th2	78	81	81	81.5	81.5
G4PE						
	Th1	56.5	60.5	61.5	62.5	63
	Th2	78.5	81	81.5	81.5	81.5

NA,not available; melting transition was not detected or well defined.

T_m, thermal unfolding midpoint.

underlined)[32–35]; these earlier findings are in good agreement with our results. It is plausible to assume that human IgG2 is more resistant than IgG1 to non-enzymatic proteolysis for the following reasons: (1) it is shorter at the hinge region; (2) the hinge region has a more rigid structure owing to the presence of four S-S bonds; and (3) the amino acid sequence of human IgG2 is distinctly different from that of human IgG1. Aggregate formation increased with decreasing pH, and the order of the total amounts of aggregates within the pH range 4.0 to 7.0 was IgG1 < IgG2 < IgG4. IgG4 was unstable in the acidic pH range. Our results are consistent with those described previously.[21,26,27,36,37] Moreover, in these previous studies the pH-dependent effects of subclass changes on the physicochemical stability of

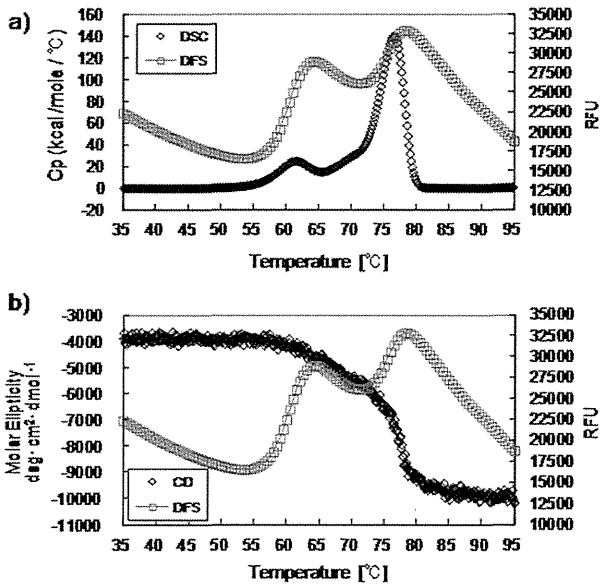

Figure 6. Comparison of thermal unfoldings of mAb-C IgG4PE at pH 5.0, as monitored by (a) DSC and DSF, and (b) CD and DSF.

antibodies were almost identical to the changes produced by each antibody variable domain reported here.

Development of antibody formulations with increased concentrations is desirable in biotherapeutics[38]; however, aggregation capacity should be carefully evaluated in the case of high-concentration formulations. It has been suggested that aggregates of antibodies might be correlated with immunogenicity.[39,40] The choice of subclass might determine the aggregation tendency of the antibodies to be constructed.

We compared the thermal unfolding of each subclass-changed mAb-C, as monitored by CD, DSC, and DSF (Fig. 6). The DSC profile for subclass-changed mAb-C showed two well-separated transitions. For multi-domain proteins such as antibodies, multiple DSC transitions usually suggest reduced inter-domain interactions. Similar to DSC, DSF was able to distinguish two separate transitions in the thermal unfolding of mAb-C. At several test pHs, the inflection point of the DSF curve corresponded to the peak of the DSC curve and the CD thermogram, with only a small onset. The small onset was expected, because DSF monitors the exposure of hydrophobic residues, whereas DSC measures the change in excess heat capacity changes (ΔCp) and CD measures the change in secondary structure. The T_h value derived from DSF was, in principle, well correlated with the onset temperature value obtained from DSC or CD. For the other three mAbs, we observed profiles identical to those of mAb-C. We therefore proposed the T_h value obtained from DSF as a parameter for evaluating the thermodynamic stability of antibodies.

DSC is one of the methods most commonly used to characterize conformational stability on the basis of differences in thermal stability.[31,41] We compared the normalized DSC thermograms of IgG molecules and DSF data (Supporting Information Fig. 6-1 to 6-3). The T_h obtained with DSF was slightly lower than the first T_m determined by DSC under all experimental conditions. At pH 4.0, the DSF profile (Supporting Information Fig. 6) seemed similar to the transition corresponding to that of the CH2 domain, which had the lowest melting temperature for these mAb molecules, as determined by DSC. The CH2 domain was more sensitive to pH changes than the other IgG domains; this was consistent with results reported previously.[42] We plotted the correlation between T_h and the CH2 unfolding temperature T_m for different molecules (Fig. 7). A linear relationship between T_h and CH2 unfolding temperature T_m was observed. The transition of the Fab domain did not vary at this pH, as analyzed by both DSC and DSF (data not shown). At higher pH values the transition of the CH2 domain overlapped with that of the Fab domain; on the other hand, Fab domain transition did not change under the pH range tested.

Direct comparison of DSF and DSC demonstrated that both methods detected the same trends in thermostability at different pH values and the same relative stabilities of the domain. T_h was consistently lower than T_m determined by DSC. We successfully cross-validated the effects of subclass changes on the structural stability of antibodies under thermal stress by using four methods. The T_h values for the CH2 domain obtained by DSF were well correlated with the onset temperatures obtained by DSC and CD, suggesting that structural perturbation of the CH2 region can be monitored by using DSF. Our evaluation of the structural stability

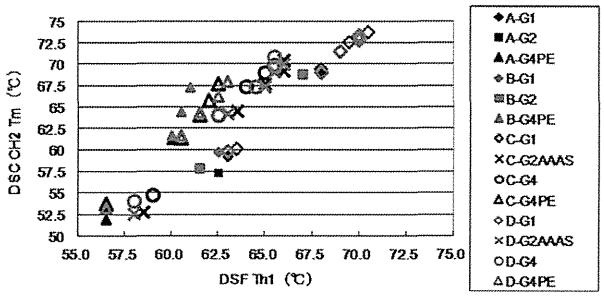

Figure 7. Correlation between DSF Th1 (temperature of hydrophobic exposure 1) and differential scanning calorimetry (DSC) CH2 T_m (thermal unfolding midpoint) values. DSF Th1 values were determined as the midpoint of the first fluorescence transition in DSF profiles by using the first derivative curves. DSC CH2 T_m values were determined as the lowest melting temperature in DSC thermograms. Linear regression yielded a linearity correlation coefficient of $r^2 = 0.9822$–0.9975.

of subclass-changed antibodies suggested that the Fc region of each subclass dominates the physicochemical characteristics of the molecules. All four molecules showed the same trend in change in structural stability, in the order of IgG1 > IgG2 > IgG4. Taken together, our findings suggest that the state of the CH2 region—the most unstable one in the domains of antibodies—is strongly correlated with the structural stability of antibodies and that aggregation tendency under acidic conditions originates from the structural stability of the CH2 domain of each subclass. Our DSF analyses suggest that exposure of the hydrophobic region upon thermal stress is correlated with the tendency of antibodies to aggregate.

Our results suggest that a tendency toward poorer physicochemical quality of antibodies is associated with the subclass type and not with the variable domain. The physicochemical properties of antibodies may therefore be conserved even if the variable domains have been exchanged with those of other IgGs. This concept might help us to select appropriate subclasses. Notably, we can exchange IgG subclasses by appropriately predicting changes in the physicochemical properties of the antibodies. Our results should provide valuable insights into antibody design using appropriate subclasses and into the process of antibody production in accordance with the physicochemical properties of different subclasses.

Materials and Methods

Materials

All IgG antibodies used were manufactured by Kyowa Hakko Kirin (Tokyo, Japan). All antibodies were expressed in Chinese Hamster Ovary cells under essentially identical conditions. Secreted antibodies were recovered from the culture medium and purified by using a series of chromatographic and filtration steps. Carbohydrate structures bound to all antibodies were confirmed by mass-spectroscopy, demonstrating that no major differences have been observed (data not shown).

Four IgG antibodies with different variable regions, mAb-A (human), mAb-B (human), mAb-C (chimeric), and mAb-D (humanized) have been used in this study. IgG4PE contained an amino acid point mutation of Ser228Pro and Leu235Glu in the heavy chain of IgG4 (EU-index numbering scheme used) to prevent half-antibody formation[43] and reduce antibody-dependent cytotoxicity.[44] IgG2AAAS contained an amino acid point mutation of Val234Ala, Gly237Ala, and Pro331Ser in the heavy chain of IgG2 to reduce effector functions.[45–47] Thus, the amino acid sequences of the light chains and VH regions in each set were identical, but their subclasses were different (IgG1, IgG2 or IgG2AAAS, IgG4, or IgG4PE). Their isoelectric points were in the range of 8–9. The antibody solution contained 10 m*M* sodium glutamate, 262 m*M* D-sorbitol, and 0.05 mg/mL polysorbate 80. Glutamate was selected from the buffer compounds commonly used in clinical antibody formulation. D-sorbitol was selected from the tonicity agents commonly used in antibody formulation. Polysorbate 80 was added to prevent protein particle formation. All excipients met the criteria of the monographs in the United States Pharmacopeia and National Formulary.

All evaluated antibodies were buffer-exchanged into formulations of the desired pH values by using a desalting column (NAP25 column, GE Healthcare U.K., Buckinghamshire, England), and their concentrations were adjusted to 5.0 mg/mL. The formulated antibody solutions were sterilized with a 0.22-μm filter, and 1 mL of each solution was placed into a sterilized USP-type 5-mL glass vial, which was sealed with autoclaved rubber stopper. The prepared samples were stored in a temperature-controlled incubator at 25 or 40°C for 1 or 3 months before SEC analysis and SDS-PAGE.

Size-exclusion high-performance liquid chromatography. To detect soluble aggregates and fragments, size-exclusion high-performance liquid chromatography was performed on an Alliance 2795 device equipped with a 2487 UV detector (Waters Corporation, Mildford, MA) and a TSK G3000SWXL 7.8 × 300 mm^2 column (Tosoh Biosep., Tokyo, Japan). Separation was performed with a mobile phase of 20 m*M* K_2HPO_4/KH_2PO_4 and 500 m*M* NaCl (pH 7.0) at a flow rate of 0.5 mL/min at a constant 25°C. A diluted sample was injected to obtain a total loading amount of 200 μg, and detection was performed at a wavelength of 215 nm. The resulting chromatograms were analyzed by integrating the area under each eluting peak by using Empower 2 Chromatography Data System software (Waters Corporation) and recorded as percentages of HMWS and LMWS.

SDS-PAGE. IgG samples were run on Novex 8% to 16% Tris-glycine 1.0 × 15-well precast SDS-PAGE gels (Invitrogen, Carlsbad, CA). All samples were diluted to 1 mg/mL or 0.1 mg/mL with formulation buffer and diluted further to 0.1 mg/mL or 0.01 mg/mL with a 4× solution consisting of 69 m*M* Tris–HCl (pH 7.0), 2.2% SDS, 0.04% bromophenol blue, and 22.2% glycerol buffer; under reducing conditions 111.1 m*M* dithiothreitol (DTT) was added to the 4× solution. The sample load was 1 μg or 0.1 μg. The molecular weight maker (Mark12: 200- to 2.5-kDa range) was purchased from Invitrogen.

Far-UV CD. The IgG formulations were diluted to 0.25 mg/mL with formulation buffer and quantified with a Jasco J-820 CD spectrometer in combination

with a Jasco PTC-423S temperature controller (Jasco International, Tokyo, Japan) in quartz cuvettes with a path length of 1 mm at 25°C. Far-UV spectra were collected by continuous scanning from 200 to 260 nm at a scanning speed of 10 nm/min, a response time of 1 s, a bandwidth of 1 nm, a sensitivity of 100 m, steps of 0.5 nm, and an accumulation of three scans. Spectra Analysis Software (Version1.53.04, Jasco) was used to background-correct the spectra for the spectrum of the respective buffer. Data were calculated as mean residue ellipticity based on mean amino acid residue weight. The mean residue ellipticity was determined as $[\theta]_{\mathrm{mrw},\,\lambda} = (\mathrm{MRW} \times \theta_\lambda)/(10 \times c \times d)$, where MRW is the mean residue weight, θ_λ is the observed ellipticity (in millidegrees) at wavelength λ, c is the protein concentration in mg/mL, and d is the path length in cm. Thermal studies were conducted by raising the temperature in 0.5°C intervals from 25 to 100°C at a rate of 60°C/h. Far-UV CD spectrum after heating have been measured by incubation of the sample at 25°C for 15 min. The molar ellipticity at 217 nm was monitored for changes in the relative content of the β-sheet structure of the immunoglobulins.

DSC. The thermal stability of individual domains was evaluated by using DSC. Measurements were performed on a 1.0 mg/mL IgG solution using a capillary VP-DSC system (MicroCal LLC, Northampton, MA) with a cell volume of 0.135 mL. Temperature scans were performed from 25 to 100°C at a scan rate of 1°C/min. A buffer–buffer reference scan was subtracted from each sample scan before concentration normalization. Baselines were created in Origin 7.0 (OriginLab, Northampton, MA) by cubic interpolation of the pre- and post-transition baselines.

DSF. DSF was used to monitor IgG unfolding during temperature melting. A 96-well microplate was used during DSF, with each well containing 19.5 μL of IgG sample and 0.5 μL of SYPRO Orange (Invitrogen Inc.) that had been diluted from the purchased stock to 1:125 in water. The final dye concentration was 1/5000 of that of the initial product. A CFX96 Real-Time PCR instrument (Bio-Rad Laboratories, Hercules, CA) was used, and the "FRET" channel setting was used to record fluorescence changes during DSF measurement. Samples were incubated at 20°C for 3 min before the melting, during which time the temperature was increased from 35 to 95°C in 0.5°C increments, with an equilibration time of 10 s at each temperature. The hydrophobic exposure temperature, T_m1 or T_m2, was reported as an indication of the transition midpoint of protein unfolding. The first-order derivative curves and T_m values were determined by using CFX Manager software (Bio-Rad Laboratories).

Acknowledgments

The authors thank Dr. Masayoshi Tsukahara and Dr. Tomoyoshi Ishikawa for fruitful discussions and Ms. Rie Sato and Ms. Kazue Sasaki for help with experimental work.

References

1. Chan AC, Carter PJ (2010) Therapeutic antibodies for autoimmunity and inflammation. Nat Rev Immunol 10: 301–316.
2. Beck A, Wurch T, Bailly C, Corvaia N (2010) Strategies and challenges for the next generation of therapeutic antibodies. Nat Rev Immunol 10:345–352.
3. Reichert JM (2012) Marketed therapeutic antibodies compendium. mAbs 4:413–415.
4. Davies DR, Metzger H (1983) Structural basis of antibody function. Annu Rev Immunol 1:87–117.
5. Cambier JC, Bedzyk W, Campbell K, Chien N, Friedrich J, Harwood A, Jensen W, Pleiman C, Clark MR (1993) The B-Cell antigen receptor: structure and function of primary, secondary, tertiary and quaternary components. Immunol Rev 132:85–106.
6. Jefferis R (2007) Antibody therapeutics: isotype and glycoform selection. Exp Opin Biol Ther 7:1401–1413.
7. Clark MR (1997) IgG effector mechanism. Chem Immunol 7:715–725.
8. Bell E (2006) Antibodies: IgG effector function: a question of balance. Nat Rev Immunol 6:4–5.
9. Salfeld JG (2007) Isotype selection in antibody engineering. Nat Biotechnol 25:1369–1372.
10. Labrijn AF, Aalberse RC, Schuurman J (2008) When binding is enough: nonactivating antibody formats. Curr Opin Immunol 20:479–485.
11. Jiang XR, Song A, Bergelson S, Arroll T, Parekh B, May K, Chung S, Strouse R, Mire-Sluis A, Schenerman M (2011) Advances in the assessment and control of the effector functions of therapeutic antibodies. Nat Rev Drug Discov 10:101–109.
12. Dall'Acqua WF, Cook KE, Damschroder MM, Woods RM, Wu H (2006) Modulation of the effector functions of a human IgG1 through engineering of its hinge region. J Immunol 177:1129–1138.
13. Yoo EM, Wims LA, Chan LA, Morrison SL (2003) Human IgG2 can form covalent dimers. J Immunol 170:3134–3138.
14. Wypych J, Li M, Guo A, Zhang Z, Martinez T, Allen MJ, Fodor S, Kelner DN, Flynn GC, Liu YD, Bondarenko PV, Ricci MS, Dillon TM, Balland A (2008) Human IgG2 antibodies display disulfide-mediated structural isoforms. J Biol Chem 283:16194–16205.
15. Dillon TM, Ricci MS, Vezina C, Flynn GC, Liu YD, Rehder DS, Plant M, Henkle B, Li Y, Deechongkit S, Varnum B, Wypych J, Balland A, Bondarenko PV (2008) Structural and functional characterization of disulfide isoforms of the human IgG2 subclass. J Biol Chem 283:16206–16215.
16. Liu YD, Chen X, Enk JZ, Plant M, Dillon TM, Flynn GC (2008) Human IgG2 antibody disulfide rearrangement in vivo. J Biol Chem 283:29266–29272.
17. Martinez T, Guo A, Allen MJ, Han M, Pace D, Jones J, Gillespie R, Ketchem RR, Zhang Y, Balland A (2008) Disulfide connectivity of human immunoglobulin G2 structural isoforms. Biochemistry 47:7496–7508.
18. Van der Neut Kolfxchoten M, Schuurman J, Losen M, Bleeker WK, Martinez-Martinez P, Vermeulen E, den Bleker TH, Wiegman L, Vink T, Aarden LA, De Baets MH, van de Winkel JG, Aalberse RC, Parren PW

(2007) Anti-inflammatory activity of human IgG4 antibodies by dynamic Fab arm exchange. Science 317: 1554–1557.
19. Van der Zee JS, van Swieten P, Aalberse RC (1986) Serologic aspects of IgG4 antibodies. IgG4 antibodies form small, nonprecipitating immune complexes due to functional monovalency. J Immunol 137:3566–3571.
20. Schuurman J, Van Ree R, Perdok GJ, Van Doorn HR, Tan KY, Aalberse RC (1997) Normal human immunoglobulin G4 is bispecific: it has two different antigen-combining sites. Immunology 97:693–698.
21. Ejima D, Tsumoto K, Fukuda H, Yumioka R, Nagase K, Arakawa T, Philo JS (2007) Effects of acid exposure on the conformation, stability, and aggregation of monoclonal antibodies. Proteins 66:954–962.
22. Franey H, Brych SR, Kolvenbach CG, Rajan RS (2010) Increased aggregation propensity of IgG2 subclass over IgG1: role of conformational changes and covalent character in isolated aggregates. Protein Sci 19:1601–1615.
23. Vermeer AW, Norder W (2000) The thermal stability of immunoglobulin: unfolding and aggregation of a multidomain protein. Biophys J 78:394–404.
24. Garber E, Demarest JD (2007) A broad range of Fab stabilities within a host of therapeutic IgGs. Biochem Biophys Res Commun 355:751–757.
25. Demarest SJ, Rogers J, Hansen G (2004) Optimization of the antibody CH3 domain by residue frequency analysis of IgG sequences. J Mol Biol 335:41–48.
26. Hari SB, Lau H, Razinkov VI, Chen S, Latypov RF (2010) Acid-induced aggregation of human monoclonal IgG1 and IgG2: molecular mechanism and the effect of solution composition. Biochemistry 49:9328–9338.
27. Latypov RF, Hogan S, Lau H, Gadgil H, Liu D (2012) Elucidation of acid-induced unfolding and aggregation of human immunoglobulin IgG1 and IgG2 Fc. J Biol Chem 287:1381–1396.
28. Andersen CB, Manno M, Rischel C, Thórólfsson M, Martorana V (2010) Aggregation of multidomain protein: a coagulation mechanism governs aggregation of a model IgG1 antibody under weak thermal stress. Protein Sci 19:279–290.
29. He F, Hogan S, Latypov RF, Narhi LO, Razinkov VI (2010) High throughput thermostability screening of monoclonal antibody formulations. J Pharm Sci 99: 1707–1720.
30. Goldberg DS, Bishop SM, Shah AU, Sathish HA (2010) Formulation development of therapeutic monoclonal antibodies using high-throughput fluorescence and static light scattering techniques: role of conformational and colloidal stability. J Pharm Sci 100:1306–1315.
31. King AC, Woods M, Liu W, Lu Z, Gill D, Krebs MR (2011) High-throughput measurement, correlation analysis, and machine-learning predictions for pH and thermal stabilities of Pfizer-generated antibodies. Protein Sci 20:1546–1557.
32. Cohen SL, Price C, Vlasak J (2007) Beta-elimination and peptide bond hydrolysis: two distinct mechanisms of human IgG1 hinge fragmentation upon storage. J Am Chem Soc 129:6976–6977.
33. Xiang T, Lundell E, Sun Z, Liu H (2007) Structural effect of a recombinant monoclonal antibody on hinge region peptide bond hydrolysis. J Chromatogr 858:254–262.
34. Cordoba AJ, Shyong BJ, Breen D, Harris RJ (2005) Non-Enzymatic hinge region fragmentation of antibodies in solution. J Chromatogr 818:115–121.
35. Gaza-Bulseco G, Liu H (2008) Fragmentation of a recombinant monoclonal antibody at various pH. Pharm Res 25:1881–1890.
36. Ishikawa T, Ito T, Endo R, Nakagawa K, Sawa E, Wakamatsu K (2010) Influence of pH on heat-induced aggregation and degradation of therapeutic monoclonal antibodies. Biol Pharm Bull 33:1413–1417.
37. Franey H, Brych SR, Kolvenbach CG, Rajan RS (2010) Increased aggregation propensity of IgG2 subclass over IgG1: role of conformational change and covalent character in isolated aggregates. Protein Sci 19:1601–1615.
38. Daugherty AL, Mrsny RJ (2006) Formulation and delivery issue for monoclonal antibody therapeutics. Adv Drug Deliv Rev 58:686–706.
39. Fradkin AH, Carpenter JF, Randolph TW (2009) Immunogenicity of aggregates of recombinant human growth hormone in mouse models. J Pharm Sci 98: 3247–3264.
40. Rosenberg AS (2006) Effects of protein aggregates: an immunologic perspective. AAPS J 8:E501–E507.
41. Ionescu RM, Vlasak J, Price C, Kirchmeier M (2008) Contribution of variable domain to the stability of humanized IgG1 monoclonal antibodies. J Pharm Sci 97:1414–1426.
42. Welfle K, Misselwitz R, Hausdorf G, Höhne W, Welfle H (1999) Conformation, pH-induced conformational changes, and thermal unfolding of anti p24 (HIV-1) monoclonal antibody CB 4–1 and its Fab and Fc fragments. Biochim Biophys Acta 1431:120–131.
43. Angal S, King DJ, Bodmer MW, Turner A, Lawson AD, Roberts G, Pedley B, Adair JR (1993) A single amino acid substitution abolishes the heterogeneity of chimeric mouse/human (IgG4) antibody. Mol Immunol 30: 105–108.
44. Reddy MP, Kinney CA, Chaikin MA, Payne A, Fishman-Lobell J, Tsui P, Dal Monte PR, Doyle ML, Brigham-Burke MR, Anderson D, Reff M, Newman R, Hanna N, Sweet RW, Truneh A (2000) Elimination of Fc receptor-dependent effector functions of a modified IgG4 monoclonal antibody to human CD4. J Immunol 164:1925–1933.
45. Cole MS, Anasetti C, Tso JY (1997) Human IgG2 variants of chimeric anti-CD3 are nonmitogenic to T cells. J Immunol 159:3613–3621.
46. Oganesyan V, Gao C, Shirinian L, Wu H, Dall'Acqua WF (2008) Structural characterization of a human Fc fragment engineered for lack of effector functions. Acta Cryst D64:700–704.
47. An Z, Forrest G, Moore R, Cukan M, Haytko P, Huang L, Vitelli S, Zhao JZ, Lu P, Hua J, Gibson CR, Harvey BR, Montgomery D, Zaller D, Wang F, Strohl W (2009) IgG2m4, an engineered antibody isotype with reduced Fc function. Mabs 1:572–579.

Appl Microbiol Biotechnol (2013) 97:8569–8580
DOI 10.1007/s00253-013-4695-2

Secretory production of single-chain antibody (scFv) in *Brevibacillus choshinensis* using novel fusion partner

Masao Tokunaga · Makoto Mizukami · Koji Yamasaki · Hiroko Tokunaga · Hiromasa Onishi · Hiroshi Hanagata · Matsujiro Ishibashi · Akira Miyauchi · Kouhei Tsumoto · Tsutomu Arakawa

Received: 24 October 2012 / Revised: 28 December 2012 / Accepted: 3 January 2013 / Published online: 20 January 2013

Abstract Halophilic β-lactamase (BLA) has been successfully used as a novel fusion partner for soluble expression of aggregation-prone foreign proteins in *Escherichia coli* cytoplasm (Appl Microbiol Biotechnol 86:649–658, 2010b). This halophilic BLA fusion technology was applied here for secretory expression in *Brevibacillus*. The "*Brevibacillus* in vivo cloning" method, recently developed by Higeta Shoyu group, for the construction and transformation of *Brevibacillus* expression vectors facilitates efficient screening of the production conditions of *Brevibacillus* expression system. Two single-chain antibodies (scFv), HyHEL-10 single chain scFv (scFvHEL) and anti-fluorescein single chain scFv (scFvFLU), were successfully secreted to culture supernatant as a fusion protein with halophilic BLA. The scFvHEL-His, purified after cleavage of BLA portion with thrombin, was fully active: it formed a stoichiometric complex with the antigen, lysozyme, and inhibited the enzymatic activity. The scFvFLU-His, similarly expressed and purified, stoichiometrically inhibited fluorescence intensity of fluorescein. The molecular mass of scFvHEL-His was determined to be 27,800 Da by light scattering measurements, indicating its monomeric structure in solution.

Keywords Halophilic β-lactamase · Single-chain antibody (scFv) · *Brevibacillus choshinensis* · Fusion protein · Net negative charge · High solubility

M. Tokunaga (✉) · K. Yamasaki · H. Tokunaga · M. Ishibashi
Applied and Molecular Microbiology, Faculty of Agriculture,
Kagoshima University, 1-21-24 Korimoto,
Kagoshima 890-0065, Japan
e-mail: tokunaga@chem.agri.kagoshima-u.ac.jp

M. Mizukami · H. Onishi · H. Hanagata · A. Miyauchi
Department of Research and Development,
Higeta Shoyu Co., Ltd, 2-8 Chuo-cho,
Choshi, Chiba 288-8680, Japan

K. Tsumoto
Medical Proteomics Laboratory, Institute of Medical Science, The University of Tokyo, 4-6-1 Shirokanedai, Minato-ku,
Tokyo 108-8639, Japan

T. Arakawa
Alliance Protein Laboratories, 3957 Corte Cancion,
Thousand Oaks, CA 91360, USA

Introduction

Proteins from halophilic bacteria function normally and remain stable in varying salt concentrations (DasSarma et al. 2006; Ventosa et al. 1998). They possess unique amino acid sequences characterized by high content of acidic amino acid residues and resultant high net negative charges at physiological pH (Elcock and McCammon 1998; Mevarech et al. 2000; Tokunaga et al. 2004; Yamaguchi et al. 2011, 2012; Yonezawa et al. 2007). These characteristics confer halophilic proteins' high aqueous solubility and resistance to aggregation at high salt concentrations. For example, β-lactamase (BLA) from *Chromohalobacter* sp. 560 was soluble both in the native and denatured state, resulting in high refolding efficiency from the denatured structures (Arakawa et al. 2010; Tokunaga et al. 2004, 2006a). Reflecting high solubility and efficient folding under variable salt concentrations, BLA was efficiently expressed as a native active protein in *Escherichia coli* cytoplasm (Tokunaga et al. 2004) despite being a secretory protein. These ideal properties of BLA have enabled us to develop a novel BLA-fusion protein expression system for soluble expression in *E. coli* (Tokunaga et al. 2010a, b).

Monoclonal antibodies occupy a large fraction of biopharmaceutical proteins (Yamada 2011). One of the disadvantages

of using the whole antibody is its large size, which limits penetration into diseased areas (Beck et al. 2010; Demarest and Glaser 2008; Kontermann 2010). Binding of Fc domain of the whole antibody to cell surface Fc receptor also limits the circulation and mobility. Smaller version of antibody, lacking Fc domains, can overcome these problems and also open an opportunity for intracellular delivery. One of them is a construct linking two variable domains, i.e., heavy and light chains, of antibody with a flexible spacer, called single-chain antibody (scFv) (Stockwin and Holmes 2003; Wörn and Plückthun 2001). Such scFv molecules normally retain the original antigen specificity and affinity. Conjugation of scFv with cytotoxic agents is intensely developed for site-specific delivery of anti-cancer agents (Beckman et al. 2007; Ottiger et al. 2009). It is increasingly apparent, however, that the mammalian secretion system, which is a major workhorse for the production of monoclonal antibodies (Chon and Zarbis-Papastoitsis 2011; Shukla and Thommes 2010) and other secretory proteins, is rather ineffective for antibody fragments due to both folding and aggregation problems (Andersen and Reilly 2004; Humphreys and Glover 2001; Ottiger et al. 2009). Thus, bacterial cells, in particular *E. coli*, have been used for production of scFv, but mostly as inclusion bodies (Andersen and Reilly 2004; Humphreys and Glover 2001). Various solubilization and refolding technologies have been developed using denaturants or detergents (Kudou et al. 2011; Lilie et al. 1998; Tsumoto et al. 2003). Such refolding technologies have been applied to various antibody fragments, often with limited success (Fujii et al. 2007; Fursova et al. 2009; Kurucz et al. 1995; Tsumoto et al. 1998). Novel expression technologies of soluble and active antibody fragments should be a valuable option for reliable production of this important class of proteins.

Brevibacillus choshinensis expression system is a well-established host–vector system for the production of foreign proteins, especially secretory proteins (Mizukami et al. 2010; Takagi et al. 1989; Yashiro et al. 2001). Recently, a simple and highly efficient cloning technique, *Brevibacillus* in vivo cloning method (BIC method), has been developed for construction and transformation of *Brevibacillus* expression vectors, making this *Brevibacillus* system more comprehensive and user friendly. We here report expression of scFv using *Brevibacillus* secretory expression system and two fusion partners, halophilic BLA or P45 that is an endogenous secretory protein of *Brevibacillus*.

Materials and methods

Bacterial strain and culture medium

B. choshinensis strain HPD31-SP3 (FERM BP-8479) was used as a host bacterium. TMN medium was used to culture transformants. The composition of TMN is as follows: 1 % glucose, 1 % Polypeptone (Nihon Pharmaceuticals, Tokyo, Japan), 0.5 % meat extract (Kyokuto Pharmaceuticals, Ibaraki, Japan), 0.2 % yeast extract (Difco, Detroit, MI, USA), 0.001 % $FeSO_4 \cdot 7H_2O$, 0.001 % $MnSO_4 \cdot 4H_2O$, 0.0001 % $ZnSO_4 \cdot 7H_2O$, pH 7.0, and 50 μg/ml neomycin.

Construction of *Brevibacillus* expression plasmids

We have tested two scFv genes, HyHEL-10 single chain scFv (scFvHEL) derived from lysozyme neutralizing monoclonal antibody (Tsumoto et al. 1994) and 4M5.3 single-chain scFv (scFvFLU) developed against fluorescein (Midelfort et al. 2004). To construct *Brevibacillus* expression plasmids, we used the BIC method, recently developed by the Department of R & D, Higeta Shoyu Co., Ltd (see detail in "Results" section). Transformation was performed according to the manufacturer's instruction (TaKaRa Code HB200). Five expression vectors (i.e., construct 1, 2, 3, 4, and 5 in Fig. 1) were constructed as follows.

pNYH5-BLA-scFvHEL-His (construct 1): vector plasmid pNYH5BLA, consisting of P5 promoter and modified secretion signal of *Brevibacillus* major cell wall protein, 6× His-tag, HaBLA, PreScission protease site, multi-cloning site, and 8× His-tag, was amplified with forward primer (Bb5BLA-F) 5′-GGATCCTGGACCTTGGAACA GAACTTCCAA-3′ and reverse primer (Bb5BLA-R) 5′-CTCGAGGAATTCCCCGGGAAGCTTCACCAT-3′. Template DNA containing scFvHEL gene was amplified with forward primer (Bb-scFv-HEL F) 5′-CAAGGTCCAGGATCCGATATCGTCCTGACCCAGAG-CCCGGCGACC-3′ and reverse primer (Bb-scFv-HEL R) 5′-GGGGAATTCCTCGAGTTAATGGTGATGGTGAT GGTGACCCGCGGA-3′.

The underlined sequences in primers are overlapped with both ends of vector sequence (B*am*HI–*Xho*I site of pNYH5BLA multi-cloning site). Both amplified fragments were transformed to competent cells and plated out to TM-neomycin plate.

pNO-BLA-scFvHEL-His (construct 2): pNO326 was used as the vector for the expression of BLA-scFvHEL-His. pNO326 is a derivative of pNY326 and has only one translation start site (pNY326 has two initiation sites placed in frame, resulting in the generation of two consecutive secretion signals that possess extra 31 amino acids in length over pNO326). The nucleotide sequence coding BLA-scFvHEL-hisx6 was amplified by PCR with the following primer set: forward (R2L6blafor), 5′-CCCATGGCTTTCGCTCAAG ACGACGCGTCGGACAG-3′; and reverse (his6rev), 5′-CATCCTGTTAAGCTTAATGGTGATGGTGATGGTG-3′. pBF-BLA-scFvHEL-CHis, BLA-fusion vector for *E. coli*, was used as the template. Both primers have 15-bp overlapping sequences (underlined) with the ends of the vector,

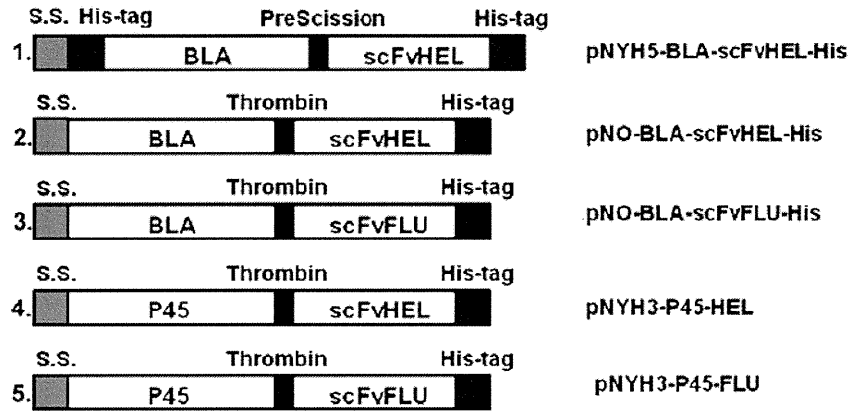

Fig. 1 Schematic illustration of scFv-expression vectors. *BLA* halophilic β-lactamase, *scFvHEL* scFv for hen egg white lysozyme, *scFvFLU* scFv for fluorescein, *S.S.* signal sequence for secretion, *His-tag* histidine tag, *PreScission* PreScission protease cleavage site, *Thrombin* thrombin cleavage site, *P45 Brevibacillus* P45 protein

resulting in recombination between the vector and the insert upon transformation.

The vector was also amplified by PCR to prepare a linearized configuration using the following primer set: forward (326for), 5′-AAGCTTAACAGGATGCGGGG GAG-3′; and reverse (R2L6rev), 5′-AGCGAAAGCCAT GGGAGCAA-3′. Both amplified fragments were transformed to competent *B. choshinensis* cells.

pNO-BLA-scFvFLU-His (construct 3): the same primer set, R2L6BLAfor and his6rev, was used to amplify the gene coding for BLA-scFvFLU-His. pBF-scFvFlu-CHis was used as the template. Other procedures were the same as those described in the preparation of pNO-BLA-scFvHEL-His construct.

pNYH3-P45-HEL (construct 4): first, P45 expression plasmid, pNYH3P45, was constructed. P45 gene was amplified from *B. choshinensis* genome with the following primer set: forward (P45for), 5′-GAACACAAGGTCATGATGAAA GGATGGAGAGAATA-3′; and reverse (P45rev), 5′-CATCCTGTTAAGCTTAATGGTGATGGTGATGGTGTT GTTCCGTCGTGGTTTCTT-3′. The amplified gene was cloned into pNY326 by BIC method to make pNYH3P45. As a next step, pNYH3P45 was linearized by PCR with the following primer set: forward (his6for), 5′-CACCATCAC CATCACCATTA-3′; and reverse (P45rev2), 5′-TTGTTCC GTCGTGGTTTCTT-3′. With the following primer set, LVPRGS (thrombin recognition sequence)-HEL gene was amplified: forward (HELthrombfor), 5′-AAGAAACC ACGACGGAACAActtgttccacgtggatccGATATCGTCCTG ACCCAGAG-3′; and reverse, his6rev.The underlined part of the forward primer corresponds to the C-terminal part of P45 and the sequence written with small letters corresponds to LVPRGS. pNO-BLA-scFvHEL-His was used as the template. The PCR product was mixed with linearized pNYH3P45 and then transformed into *B. choshinensis* competent cells.

pNYH3-P45-FLU (construct 5): with the following primer set, LVPR-scFvFlu gene was amplified: forward (Fluthrombfor), 5′-AAGAAACCACGACGGAACAA cttgttccacgtggatccGATGTGGTGATGACCCAGAC-3′; and reverse, his6rev. pNO-BLA-scFvFLU-His was used as the template. The other procedures were the same as those used for pNYH3P45-scFvHEL-His construction.

Expression and purification of scFv fusion and scFv proteins

Expression of *Brevibacillus* transformants was carried out in test tube culture (3 ml), flask batch culture (~200 ml), or controlled jar fermenter culture (2 l). Cells were grown in TM-neomycin medium in a test tube or flask for 2–3 days at 30 °C with gentle shaking, and culture supernatant was collected by centrifugation. The scFv-His fusion proteins and scFv-His proteins derived, upon protease cleavage, from fusion proteins were purified by immobilized metal affinity chromatography (Ni-NTA, Novagen and His-Trap, GE Healthcare) using 50 mM sodium phosphate buffer, pH 7.4, containing 0.15 M NaCl (PN buffer) as a standard buffer solution. Culture supernatant was mixed with an equal volume of 2-fold concentrated PN buffer and directly applied to His-Trap column, equilibrated with PN buffer, at a flow rate of 1–2 ml/min. After extensive washing of the column with PN buffer, proteins were eluted in stepwise manner with PN buffer containing 20, 50, 100, 200, and 300 mM imidazole. Fractions containing scFv fusion proteins (eluted in 100–200 mM imidazole) were collected and dialyzed against thrombin buffer (50 mM Tris–HCl buffer, pH 8.0, 0.1 M NaCl, and 0.5 mM $CaCl_2$). The dialyzed sample was digested with bovine thrombin (GE Healthcare) at 22 °C for 16 h and then applied to Ni-NTA column equilibrated with PN buffer. The bound scFv-His protein was eluted with PN buffer containing imidazole in a stepwise manner (20, 50, 100, 200, and 300 mM).

Size exclusion chromatography (SEC) and SEC–multi-angle laser light scattering (MALS) experiments

SEC analysis was performed using Superdex 75 10/300 GL column (1 × 30 cm; GE Healthcare, Uppsala, Sweden) with

0.1 M Na–phosphate buffer, pH 6.8, containing 0.2 M arginine as a standard buffer solution at a flow rate of 0.8 ml/min. Arginine has been shown to prevent non-specific binding of proteins to the SEC column (Ejima et al. 2005).

Molecular mass determination by SEC–MALS was carried out at 25 °C with Superdex 75 10/300 GL column with 0.1 M phosphate buffer, pH6.8, supplemented with 0.2 M arginine (here arginine refers to arginine hydrochloride) at a flow rate of 0.8 ml/min. The eluting solution from the SEC column was monitored by DAWN-Heleos II multi-angle laser light-scattering detector (Wyatt Technology, Santa Barbara, CA, USA) and UV detector at 280 nm (Hitachi L2400, Tokyo, Japan). The UV absorbance was converted to the protein concentration based on the extinction coefficient of 2.2 cm^2mg^{-1}. Data collection and processing were performed using the Wyatt Technology ASTRA 5 software version 5.3.4. Scattering data obtained at 18 angles were used to construct the Debye plots by Zimm's method (Andersson et al. 2003).

Antibody activity assay for scFvHEL and scFvFLU proteins

Hen egg white lysozyme (0.043 nmol) was incubated with purified scFvHEL-His protein or purified scFvHEL-His fusion protein (BLA or P45 fusion) at different molar ratios at 25 °C for 1 h. After incubation, the cell lytic activity of lysozyme was measured as follows. *Micrococcus lysodeikticus* cell suspension (A_{450}=~0.9) in 50 mM Na–phosphate buffer, pH 6.4, was mixed with enzyme solution in a cuvette placed in a photometer. The lysis of *M. lysodeikticus* cells was monitored from turbidity decrease at 450 nm. It has been demonstrated that the HyHEL-10, from which scFvHEL was derived, stoichiometrically binds to lysozyme and thereby inhibits its activity (Tsumoto et al. 1994). Binding of scFvFLU to fluorescein was examined as follows. Fluorescein (final concentration of 0.6 μM) was added into 200 μl of 0.1 M Tris–HCl buffer, pH 7.4, containing scFvFLU-His or its fusion proteins at different molar ratios, and incubated at 25 °C for 1 h. After incubation, fluorescence intensity was measured with excitation at 480 nm and emission at 515 nm by a microtiter plate reader (Infinite M200 FA). The scFvFLU (4 M5.3) binds to fluorescein and inhibits fluorescence emission (Kudou et al. 2011). All results shown here are an average of two to three independent experiments with a deviation less than 10 %.

Others

SDS–polyacrylamide gel electrophoresis (SDS–PAGE) was done according to Laemmli (Laemmli 1970). Protein concentration was measured, unless described otherwise, by bicinchonic acid method (Smith et al. 1985) and Pierce 660 nm protein assay reagent (Thermo Scientific, Rockford, IL, USA).

Results

Construction of expression vectors for scFv fusion proteins

We have examined the expression of two scFv genes, HyHEL-10 single-chain scFv and anti-fluorescein single-chain scFv. *Brevibacillus* expression plasmids were constructed based on the BIC method. Both linearized vector and target gene DNA were amplified by PCR with addition of short overlapping sequences (~15 bp) between vector and insert gene at 5′ and 3′ ends, and both fragments were transformed at once to *Brevibacillus* competent cells. The homologous recombination in *Brevibacillus* cells between overlapping sequences at 5′ and 3′ ends of vector and target gene fragments produces whole expression vector (target-gene-inserted vector) in vivo. Once several linearized vector DNA cassettes with different promoters and secretion signals were prepared, target gene amplified with short overlapping sequences of 5′ and 3′ ends of vector sequence was readily inserted to construct a series of expression vectors. Highly efficient vector construction was obtained by this BIC method: DNA sequencing data verified that more than 80 % of isolated transformants on neomycin-selection plate harbored correct plasmid which had been formed by in vivo recombination between vector and insert DNA fragments.

Several constructs were explored for expression of two scFv, as summarized in Fig. 1. They all contain signal sequence (S.S.) to direct extracellular expression and proteolytic cleavage site for either PreScission or thrombin digestion. The C-terminal His-tag can be used to purify scFv after proteolytic removal of the N-terminal fusion partner. Two fusion partners were inserted N-terminal to the scFv to enhance soluble expression, i.e., halophilic BLA and *Brevibacillus* P45 protein. P45 is a soluble secretory protein of *Brevibacillus*. Although its function is totally unknown, it appears to be a stress protein, as seen in elevated level under stress conditions. Even under normal conditions, its secretion efficiency is high. Both high solubility and expression may lead to efficient soluble expression of target proteins when fused to P45, making it a potential fusion partner.

Expression and purification of BLA-fusion protein and scFv after cleavage with protease

First three BLA-fusion constructs, i.e., construct 1, 2, and 3 described in Fig. 1, were expressed in test tube cultures along with the vector control. Figure 2a shows the SDS–PAGE of the culture supernatant fraction. The expected molecular mass of these three constructs are at ~70 kDa. As expected, vector control showed no prominent band at 70 kDa, which should make identification of expressed fusion protein easier. With these three constructs, a band at ~70 kDa is clearly seen (shown by dots), indicating that these fusion proteins are

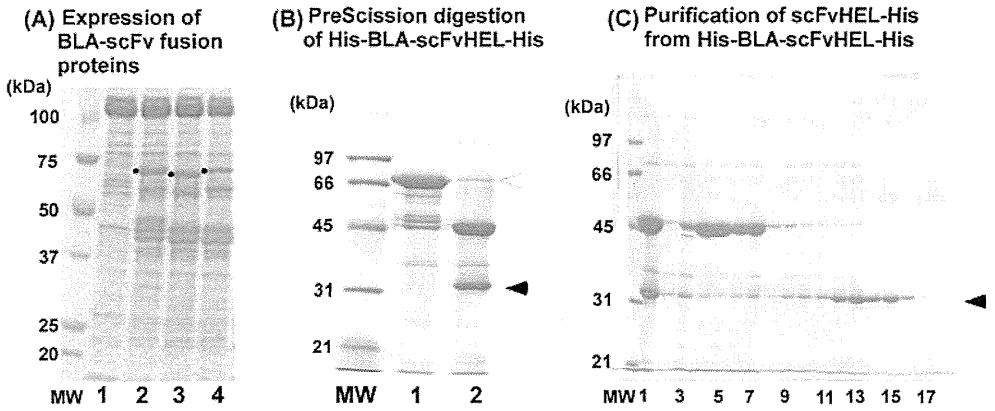

Fig. 2 Expression of BLA-scFv fusion proteins. **a** Expression of BLA-scFv fusion proteins in test tube culture. Cells were grown in 3 ml culture medium in test tube at 30 °C for 3 days. *Lane 1* negative control with blank vector, pNO326; *2* pNYH5-BLA-scFvHEL-His; *3* pNO-BLA-scFvHEL-His; *4* pNO-BLA-scFvFLU-His. *Dot* shows fusion proteins expressed. Each 4 μl of culture supernatant was applied. **b** Thrombin digestion of purified His-BLA-scFvHEL-His fusion protein. *Lane 1* partially purified fusion protein with His-Trap column, *2* after PreScission digestion. *White arrowhead*—fusion protein; *black arrowhead*—scFvHEL-His protein. **c** Purification of scFvHEL-His from PreScission-digested fusion protein with Ni-NTA column. *Black arrowhead*—scFvHEL-His protein. In this chromatography, 50 mM Tris–HCl, pH 8.0, was used instead of standard PN buffer. *Lane 1* sample of before column, *2–5* washed fraction. Imidazole-eluted fractions, 10 mM (*lanes 6–8*), 20 mM (*lanes 9–11*), 50 mM (*lanes 12–14*), and 100 mM (*lanes 15–17*), are shown

expressed in culture supernatant fractions. There appear to be a few proteins that are also expressed with the constructs, perhaps corresponding to the fragments of the fusion proteins or *Brevibacillus* proteins induced by the expression of heterologous proteins. It should be noted here that a greater mass of the fusion makes easier detection on staining than the expression of smaller scFv alone.

An attempt was made to purify BLA-fusion protein encoded on construct 1 from the culture supernatant by His-Trap column using a stepwise imidazole elution. Figure 2b (lane 1) shows the SDS–PAGE of the partially purified fraction, indicating that the 70-kDa band corresponding to His-BLA-scFvHEL-His protein (white arrowhead) was highly enriched in this fraction. This fraction was digested with PreScission protease, resulting in cleavage into 45-kDa and 31-kDa bands (lane 2), corresponding to His-BLA and scFvHEL-His (black arrowhead). His-BLA (39.8 kDa) apparently migrated as a ~45 kDa protein. Such an unusual slow mobility on SDS–PAGE has been seen in many halophilic proteins and is due to aberrant SDS binding (Tokunaga et al. 2006b, 2008). The protease digested fraction was further purified by Ni-NTA column using stepwise imidazole elution. As shown in Fig. 2c, the earlier eluting fractions from the column (lane 4 to lane 7) contained His-BLA and the later fractions contained scFvHEL-His (lane 12 to lane 15, black arrowhead). It appears that scFvHEL-His binds more strongly to Ni-NTA than His-BLA and is thus fairly free from the latter protein.

Brevibacillus jar fermenter culture and purification of scFv fusion and scFv proteins

Having established above that BLA-fusion produces protease cleavable scFvHEL protein, construct 2 and 3 that lack the N-terminal His-tag was expressed in controlled jar fermenter culture of *Brevibacillus*. Figure 3a shows the SDS–PAGE of the culture supernatant (each 1 μl was applied) in which BLA-scFvHEL-His (lane 2, shown by white arrowhead) and BLA-scFvFLU-His (lane 1, black arrowhead) were clearly expressed around 70 kDa. The amount of fusion proteins secreted was estimated to be ~0.5 mg/ml judged by the band intensity of SDS–PAGE. The resultant culture supernatant was applied to His-Trap column as described in the "Materials and methods" section. Purified BLA-scFvHEL-His was subjected to thrombin digestion and then Ni-NTA chromatography. Figure 3b shows SDS–PAGE of fractions eluted by stepwise imidazole elution. In this case, BLA eluted in early fractions (lanes 2 and 3), as expected from no N-terminal His-tag for this construct. The later fractions contained relatively pure scFvHEL-His (lane 12 to lane 17). Fractions 15 and 16 were pooled for subsequent analysis. The final products of purified BLA-scFvHEL-His fusion and scFvHEL-His proteins are shown in Fig. 3c, lanes 1 and 2, indicating purification to homogeneity.

A similar experiment, i.e., His-Trap purification of the fusion protein, thrombin cleavage, and Ni-NTA purification of the cleaved scFvFLU-His, was done for BLA-scFvFLU-His construct (construct 3) and the results are shown in Fig. 3d in which fairly pure preparations of BLA-scFvFLU-His (lane 1) and scFvFLU-His (lane 2) were also obtained. However, it should be noted that this construct showed batch dependence of product quality and hence more work is required for optimal cell culture conditions. The problem appears to be due to greater aggregation tendency of scFvFLU protein.

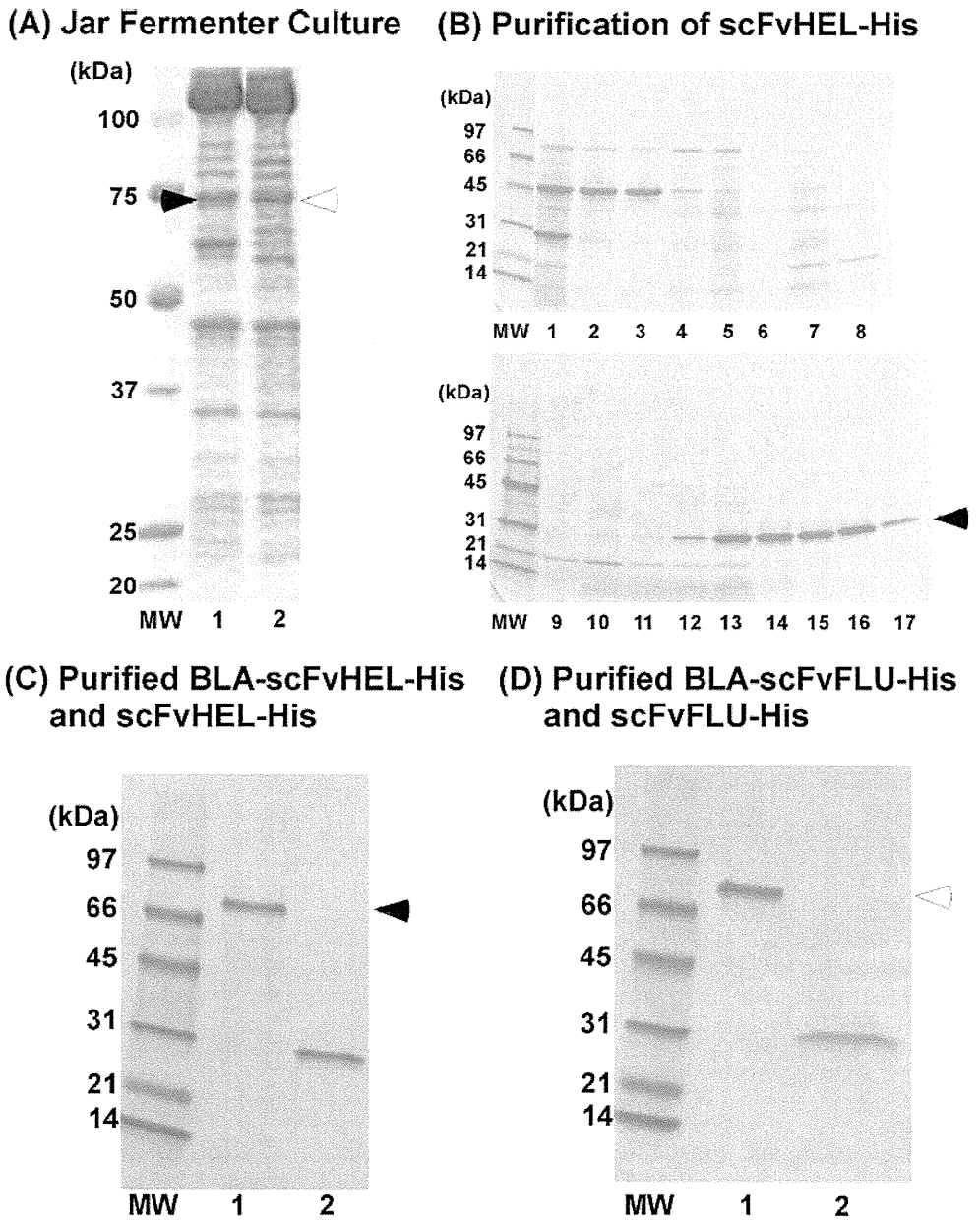

Fig. 3 Expression and purification of scFv proteins from jar fermenter culture. **a** Expression of BLA-scFvHEL-His (*white arrowhead*, *lane 2*) and BLA-scFvFLU-His (*black arrowhead*, *lane 1*) in culture supernatant of *Brevibacillus* jar fermenter culture. Each 1 μl was applied to SDS–PAGE. **b** Purification of scFvHEL-His protein with Ni-NTA column after digestion of fusion protein. *Black arrowhead*—scFvHEL-His. *Lane 1* thrombin-digested fusion protein before column; *lanes 2–17* represent fractions of Ni-NTA column, flow through (*2*), 20 mM (*3–5*), 50 mM (*6–8*), 100 mM (*9–11*), 200 mM (*12–14*), and 300 mM (*15–17*) imidazole-eluted fractions. **c** Purified BLA-scFvHEL-His (*lane 1*, *black arrowhead*) and scFvHEL-His (*lane 2*) proteins. **d** Purified BLA-scFvFLU-His (*lane 1*, *white arrowhead*) and scFvFLU-His (*lane 2*) proteins

SEC and SEC–MALS analysis

These scFv-His proteins purified to homogeneity (Fig. 3b, lanes 15–16; Fig. 3c and d, lane 2) from the BLA-fusion construct were analyzed by SEC on Superdex 75 using 0.1 M Na–phosphate buffer (pH 6.8)/0.2 M arginine mobile phase. As shown in Fig. 4a, a single peak of scFvHEL-His was observed (upper panel), with no apparent peaks corresponding to aggregated species and consistent with the purity observed in SDS–PAGE (Fig. 3c). Figure 4a (lower panel) shows SEC analysis of scFvFLU-His with a main peak (III), corresponding to scFvFLU-His. A few minor peaks (I and II) were seen in this sample, perhaps corresponding to oligomers. The observed oligomers are consistent with the aggregation tendency of the scFvFLU protein and consequent batch-dependent product quality variation as described above. The retention times for two scFv proteins (peak I in upper panel and peak III in lower panel) were very similar (14.4 min and 14.6 min), consistent with the similar molecular weight.

The monomeric state of the scFvHEL-His in aqueous solution was confirmed by SEC–MALS technique. As shown in Fig. 4b, the elution profile (upper panel, A_{280}) is similar to the result shown in Fig. 4a, showing one major peak with a shoulder before the peak. The lower panel shows the light scattering intensity of the eluted peaks. The molecular mass of the main absorbance peak was determined to be 27,800 Da, consistent with the theoretical molecular mass (26,495 Da), indicating a monomeric structure of scFvHEL-His. A large light scattering peak was also

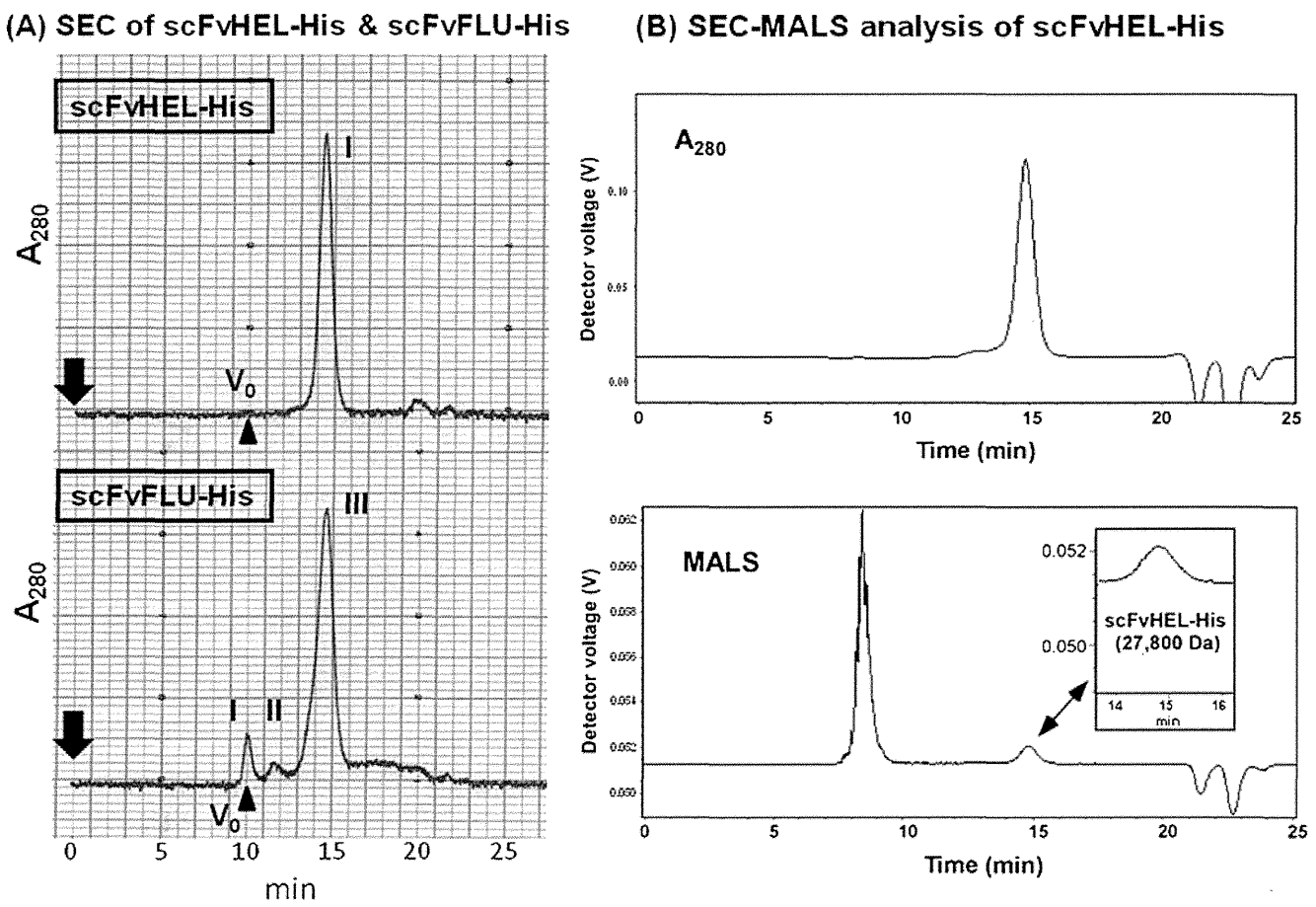

Fig. 4 Size-exclusion chromatography and light scattering analysis of scFv-His proteins. **a** Superdex 75 SEC analysis of scFvHEL-His (*upper panel*) and scFvFLU-His (*lower panel*). *Arrow* shows start point of chromatography. V_0 shows void volume. Peak I (retention time, 14.4 min) in *upper panel* shows monomer peak of scFvHEL-His. Peak III (retention time, 14.6 min) in *lower panel* shows monomer peak of scFvFLU-His. Peaks I and II show a small amount of aggregations of scFvFLU-His. **b** SEC–MALS analysis of scFvHEL-His protein. *Upper panel* shows A_{280} signal and *lower panel* shows light scattering signal. In the *lower panel*, the peak region corresponding to the scFv monomer was expanded in inserted figure

observed at the void volume (lower panel), where a small drift of A_{280} base line was observed (upper panel). This is simply due to the fact that light scattering intensity is proportional to the molecular weight and hence even small amounts of large aggregates can generate strong light scattering signals. Thus, it can be concluded that some aggregates are present in this scFvHEL-His preparation, but in negligible amounts (as seen in A_{280} profile). A similar retention time of peak III in Fig. 4a (lower panel) to the retention time for scFvHEL-His suggests that a majority of scFvFLU-His preparation is also monomeric in solution.

Antibody activity assay of scFvHEL-His and scFvFLU-His proteins

The effects of scFvHEL-His on lysozyme activity were examined based on inhibition of the enzyme activity and formation of their complex. Figure 5a shows titration curve of lysozyme activity as a function of scFvHEL-His concentration. As the scFvHEL-His concentration was increased at the fixed concentration of lysozyme, the enzyme activity was gradually reduced (from right to left). When the ratio of scFvHEL-His to lysozyme was 0.5, the lysozyme activity was reduced to half and the activity was negligible at the ratio of 1. Thus, binding of scFvHEL-His to lysozyme is nearly stoichiometric and of high affinity. It is evident that scFvHEL-His binds to lysozyme in a manner that causes blocking of enzyme active site. Binding of scFvHEL-His to lysozyme was confirmed by SEC analysis. Figure 5b shows SEC analysis of 1:1 molar ratio mixture of scFvHEL-His and lysozyme. Figure 5b [bottom panel (C)] shows the elution of lysozyme (black arrow), while the middle panel (B) shows the elution position of scFvHEL-His (white arrow). When they were mixed [upper panel (A)], the lysozyme peak (black arrow) disappeared, suggesting that it was incorporated into a complex with scFvHEL-His. The peak position of scFvHEL-His (peak II) was also moved to smaller elution position, indicating binding of lysozyme. Based on fairly small shift of elution position, the